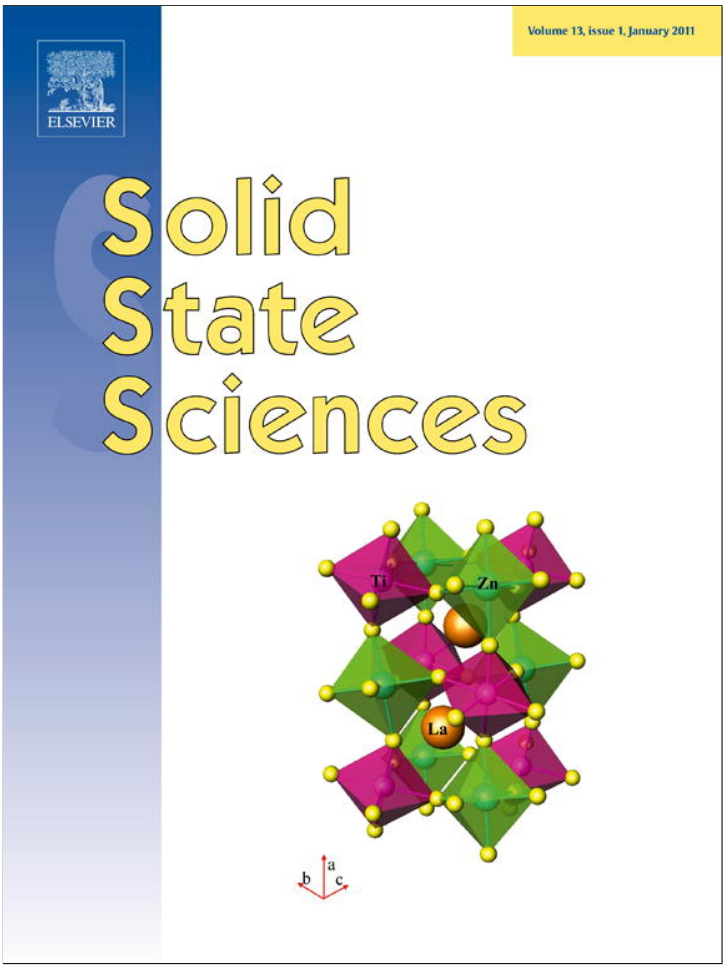

(This is a sample cover image for this issue. The actual cover is not yet available at this time.)

Solid State Sciences 14 (2012) 375–380

Contents lists available at SciVerse ScienceDirect

Solid State Sciences

journal homepage: www.elsevier.com/locate/ssscie

Electronic structure and chemical bonding of LiYSi

Samir F. Matar [a,*], Rainer Pöttgen [b], Naïm Ouaini [c]

[a] CNRS, Université de Bordeaux, ICMCB, 87 Avenue du Docteur Albert Schweitzer, 33600 Pessac, France
[b] Institut für Anorganische und Analytische Chemie, Universität Münster, Corrensstrasse 30, D-48149 Münster, Germany
[c] Université Saint Esprit de Kaslik (USEK), Faculté des Sciences, URA GREVE (CNRS/USEK/UL), Jounieh, Lebanon

ARTICLE INFO

Article history:
Received 16 November 2011
Received in revised form
8 December 2011
Accepted 9 December 2011
Available online 16 December 2011

Keywords:
Lithium
DFT
Crystal chemistry
Chemical bonding

ABSTRACT

The electronic structure of the ternary silicide LiYSi (ZrNiAl type, $P\bar{6}2m$ N°189, $a = 702.3$, $c = 421.2$ pm) is examined from ab initio with an assessment of the properties of chemical bonding. The compound is found semi-conducting with a very small gap and the chemical bonding is found mainly between Y and Si as well as Li–Si with differentiated Li–Si1/Li–Si2. The structure with totally de-intercalated Li keeps the characteristics of LiYSi with a reduction of the c/a ratio and of the volume albeit with less stability than binary YSi with orthorhombic CrB type structure. The electronic structure calculations indicate the possibility of an at least partial delithiation $Li_{1-x}YSi$ while keeping the hexagonal structure.

1. Introduction

Silicon based lithiated compounds were thoroughly studied in recent years with respect to their use as electrode materials in lithium-ion batteries [1,2], since such anodes have much higher gravimetric energy density and volumetric capacity than carbon based ones. Due to crystalline-to-amorphous phase transitions of the diverse Li_xSi phases the mechanisms of silicon lithiation and delithiation processes are still not completely understood. The silicide $Li_{15}Si_4$ was found to be the fully electrochemically lithiated phase of Si (crystalline or amorphous) [3]. Besides the mechanistic problems, the high sensitivity against traces of water hampers the broad use of the binary silicides. Nevertheless, especially $Li_{12}Si_7$ has highly interesting basic properties, i.e. different dimensionality for the crystallographically different lithium sites and aromaticity for the silicon pentagons [4–6].

Higher hydrolysis stability has been observed for ternary silicides $Li_xT_ySi_z$ (T = transition metal), where the lithium atoms fill channels or cages within two- or three-dimensional $[T_ySi_z]^{\delta-}$ polyanionic networks. An overview on the structural chemistry and the lithium mobility of these materials has been given recently [7]. An interesting compound of this structural family is $LiRh_2Si_2$ [8], which crystallizes with a site occupancy variant of U_3Si_2. Interestingly LiY_2Si_2 and $LiNd_2Si_2$ [9] are isopointal with $LiRh_2Si_2$ [8]. The distinct differences in chemical bonding between $LiRh_2Si_2$ and LiY_2Si_2 have been studied thoroughly on the basis of ab initio electronic structure calculations [8].

In contrast to the large number of $Li_xT_ySi_z$ phases [7], the family of ternary rare earth metal (RE) based silicides $Li_xRE_ySi_z$ has only scarcely been studied. Besides LiY_2Si_2 and $LiNd_2Si_2$ [9] only LiYSi [10], $Li_{0.34}CeSi_{1.66}$, LiCeSi, $LiCeSi_2$ [11], $LiEu_2Si_3$ [12], $Li_{0.75}Gd_{0.75}Si_{1.5}$ [13], and the series $Li_2RE_2Si_3$ (RE = La, Ce, Pr, Nd, Sm) [11,14,15] have been reported. These studies mainly focussed on the phase formation and structural chemistry. Some magnetic properties have been studied for the $Li_2RE_2Si_3$ series [15]. $Li_2Ce_2Si_3$ is a remarkable compound since its Curie temperature of 17 K is among the highest for cerium based intermetallics.

In extension of our systematic phase analytical studies on $Li_xT_ySi_z$ phases [7] we have recently reinvestigated $Li_2La_2Si_3$ [16] which is a Zintl phase with an electron partition $(2La^{3+})(2Li^{+})(2Si1^{2-})(Si2^{4-})$. Solid state ^{7}Li and ^{29}Si MAS-NMR spectra resolved the crystallographically independent lithium and silicon sites. Electronic structure calculations in line with strong Knight shift contributions in the observed ^{29}Si resonance shifts indicate variance with the Zintl concept. Based on these results we were motivated to study the bonding peculiarities on the other silicides. Also LiYSi [10] with ZrNiAl type structure can be described with an electron partition $Li^{+}Y^{3+}Si^{4-}$, considering Si^{4-} Zintl ions. Besides the characterization on the basis of X-ray single crystal data, no further studies have been performed on LiYSi. In continuation of our work on $Li_2La_2Si_3$ we report herein on the electronic

* Corresponding author. Tel.: +33 5 4000 2690; fax: +33 5 4000 2761.
E-mail addresses: matar@icmcb-bordeaux.cnrs.fr (S.F. Matar), pottgen@uni-muenster.de (R. Pöttgen), naimouaini@usek.edu.lb (N. Ouaini).

1293-2558/$ – see front matter © 2011 Elsevier Masson SAS. All rights reserved.
doi:10.1016/j.solidstatesciences.2011.12.009

Table 1
Experimental and calculated lattice parameters of LiYSi {Si1 (1*a*) (0, 0, 0) and Si2 (2*d*) (1/3 2/3 1/2)} and YSi; FU: formula unit.

LiYSi, $P\bar{6}2m$, $Z = 3$	LiYSi exp. [10]	LiYSi calc.	Li-free LiYSi calc.
a (Å)	702	703	695
c (Å)	421	421	407
V (nm^3)	0.1799	0.1805	0.1704
V (nm^3)/FU	0.0600	0.0602	0.0568
Li (3*g*) (*x*, 0, ½)	$x = 0.229$	$x = 0.232$	–
Y (3*f*) (*x*′, 0, 0)	$x' = 0.575$	$x' = 0.576$	$x' = 0.569$
Energy (eV)	–	−46.88	−36.10
		−15.63/FU	−12.03/FU
YSi, *Cmcm*, $Z = 4$	YSi exp. [21]	YSi calc.	
a (pm)	425	427	
b (pm)	1052	1060	
c (pm)	382	380	
V (nm^3)	0.1708	0.1733	
V (nm^3)/FU	0.0427	0.0433	
Y (4*c*) (0, *y*, ¼)	$y = 0.146$	$x = 0.143$	
Si (4*c*) (0, *y*′, ¼)	$y' = 0.440$	$y' = 0.424$	
Energy (eV)	–	−54.24	
		−13.59/FU	

structure and the properties of chemical bonding and delithiation of LiYSi, within the quantum theoretical framework of the density functional theory (DFT) [17,18].

2. Computational methodology

We use two computational methods within the DFT in a complementary manner. The Vienna ab initio simulation package (VASP) code [19,20] allows geometry optimization. For this we use the projector augmented wave (PAW) method [21], built within the generalized gradient approximation (GGA) scheme following Perdew, Burke and Ernzerhof (PBE) [22]. The conjugate-gradient algorithm [23] is used in this computational scheme to relax the atoms. The tetrahedron method with Blöchl corrections [21] as well as a Methfessel–Paxton [24] scheme were applied for both geometry relaxation and total energy calculations. Brillouin-zone (BZ) integrals were approximated using the special *k*-point sampling of Monkhorst and Pack [25]. The optimization of the structural parameters was performed until the forces on the atoms were less than 0.02 eV/Å and all stress components less than 0.003 eV/Å^3. The calculations are converged at an energy cut-off of 250 eV for the plane-wave basis set with respect to the *k*-point integration with a starting mesh of $4 \times 4 \times 4$ up to $8 \times 8 \times 8$ for best convergence and relaxation to zero strains.

Then all-electron calculations, equally based on the DFT with the GGA-PBE functional [22], are carried out for a full description of the electronic structure and the properties of chemical bonding. They are performed using the full potential scalar-relativistic augmented spherical wave (ASW) method [26,27]. In the ASW method, the wave function is expanded in atom-centered augmented spherical waves, which are Hankel functions and numerical solutions of Schrödinger's equation, respectively, outside and inside the so-called augmentation spheres. In the minimal ASW basis set, we chose the outermost shells to represent the valence states and the matrix elements were constructed using partial waves up to $l_{max} + 1 = 3$ for Y and Si and $l_{max} + 1 = 2$ for Li. Self-consistency was achieved when charge transfers and energy changes between two successive cycles were below 10^{-8} and 10^{-6} eV, respectively. The Brillouin-zone integrations were performed using the linear tetrahedron method within the irreducible wedge [23]. The calculations are carried out assuming spin degenerate configuration. Besides the site projected density of states, we discuss qualitatively the pair interactions based on the overlap population analysis with the crystal orbital overlap population (COOP) [28]. In the plots, positive, negative, and zero COOP magnitudes indicate bonding, anti-bonding, and non-bonding interactions, respectively. We note that another scheme for describing the chemical, the ECOV (covalent bond energy) criterion based on both the overlap and the Hamiltonian populations is also accessible within the ASW method [27]. It provides similar qualitative results to the COOP.

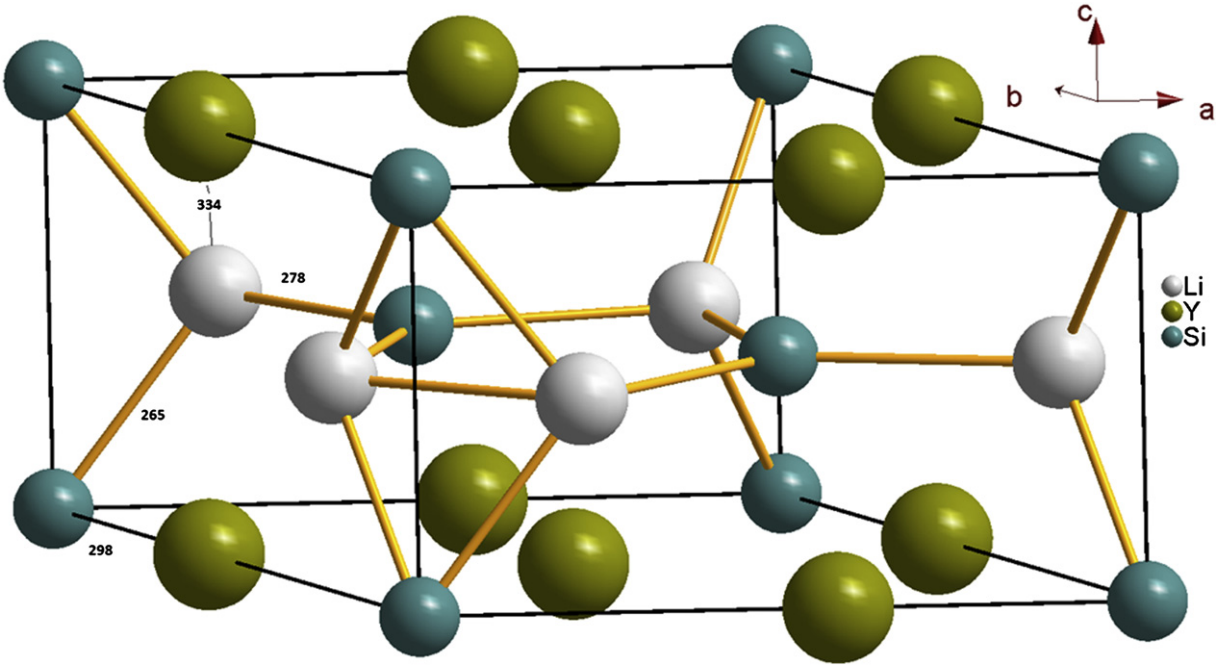

Fig. 1. The hexagonal structure of LiYSi with characteristic distances in units of pm.

3. Results of geometry optimizations, energies and electron localization

Before discussing the electronic structure of LiYSi we briefly comment on the crystal chemical peculiarities. The hexagonal structure (Table 1) of LiYSi [10] is sketched in Fig. 1. LiYSi crystallizes with the hexagonal ZrNiAl type structure, space group $P\bar{6}2m$. Along the *c* axis it consists of a succession of (Y, Si1)–(Li, Si2)–(Y, Si1) layers, separated by half a translation period. The shortest interatomic distances occur for Li–Si (265–278 pm), slightly longer than the sum of the covalent radii of 240 pm [29]. Similar Li–Si distances occur in the binary lithium silicides [30] and also in the diverse $Li_xT_ySi_z$ phases [7]. One can only ascribe medium bonding character to these interactions. The yttrium atoms are surrounded by the three-dimensional network formed by lithium and silicon. The bonding to this network proceeds via Y–Si contacts. The Y–Si distances range from 297 to 299 pm, also slightly longer than the sum of the covalent radii of 273 pm [29]. The shortest Li–Li distances of 279 pm are somewhat smaller than in *bcc* lithium (304 pm) [31], similar to the situation in $LiRh_2Si_2$ (275 pm) [8] and $Li_{13.7}Rh_8Si_{18.3}$ (268 pm) [32]. In view of the highly ionic character (and thus small size) of lithium in LiYSi (vide infra), these interactions may not be considered as bonding.

Geometry optimization was carried out for LiYSi starting with the literature data [10]. Further for the sake of establishing comparisons, similar studies were done on YSi [33]. Table 1 provides the crystal structure characteristics of the studied compounds. The geometry optimized lattice parameters and atomic positions are found in good agreement with the experiments. The slightly larger calculated volumes are due to the GGA functional which tends to overestimate lattice spacing, being 'underbinding', while the other major DFT functional, the local density approximation (LDA [34]) is 'overbinding'. Nevertheless, the differences between the experimentally determined data and those obtained from geometry optimization are small and do not affect the conclusions drawn from the subsequent calculations. For the following discussion the experimental data were used.

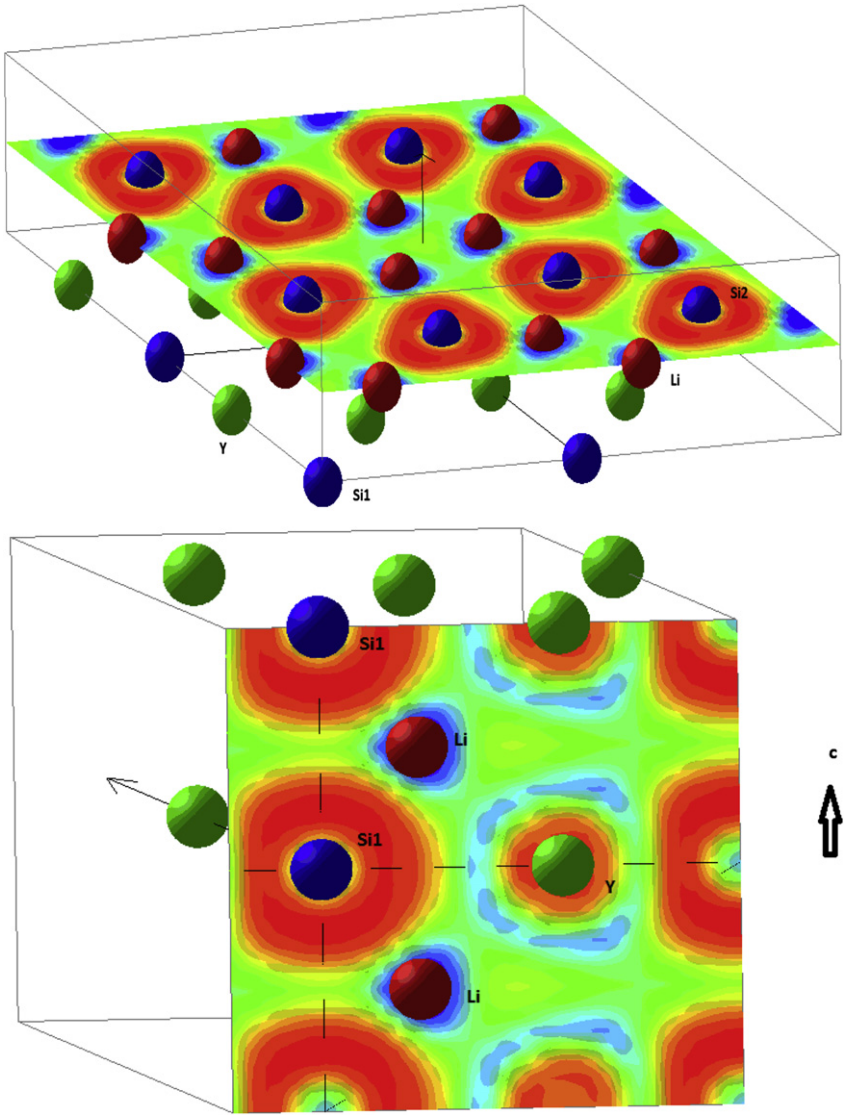

Fig. 2. LiYSi: Electron localization function (ELF) plots for a horizontal plane at $z = 1/2$ showing contours around Li and Si2 (top) and for a vertical plane containing Li, Y and Si1 (bottom). Blue, green and red contour areas designate weak, free electron-like and strong electron localizations, respectively (see text). (For interpretation of the references to color in this figure legend, the reader is referred to the web version of this article.)

In order to examine the effect of lithium de-intercalation, a hypothetic Li-free LiYSi that we designate by $\square_{Li}$YSi ($\square_{Li}$ is a vacancy of Li) was calculated based on the LiYSi structure. The results are given in the last column of Table 1. The full geometry relaxation keeps the hexagonal structure within space group $P\bar{6}2m$ and the Si atomic positions with a slight deviation. The major changes occur for the cell volume which is reduced by ~10 Å^3 for three lithium vacancies and the reduction of the hexagonal c/a ratio from 0.599 to 0.586. The total energy values per formula unit (FU) of $\square_{Li}$YSi and experimentally observed YSi (CrB type, space group *Cmcm*) given in Table 1 show that the hypothetic compound is much less stable with 1.56 eV energy difference per FU. Then such a hypothetic binary should be considered as a metastable compound. The obtained energies can be used to access the free energy. For this purpose we further calculate Li metal with the same potentials and method to obtain a total energy per atom of −1.909 eV. Then the Gibbs free energy change in the intercalation/de-intercalation process of LiYSi per formula unit (FU) is:

$$\Delta G = E(\text{LiYSi}) - E(\text{Li}) - E(\square_{Li}\text{YSi}) = -1.691 \text{ eV}.$$

The (absolute) value is larger than the one obtained for $Li_{15}Si_4$: $\Delta G = -1.136$ eV [3]. It corresponds, with inverse sign, to the average intercalation voltage, *V* which is found intermediate between the highest intercalation voltages for the Li intercalation compounds $LiMO_2$ (M = 3*d* transition metal) [35] with values amounting to ~3–4 V and Li_xSi binaries such as $Li_{15}Si_4$ with ~0.30 V [3]. Then LiYSi is intermediate between oxide intercalation compounds and binary Li_xSi due to the partial ionic character brought in by the presence of yttrium within a {LiSi} substructure.

The electron localization is illustrated with the function ELF [36] obtained from real space calculations: ELF = $(1 + \chi\sigma^2)^{-1}$. In this expression the ratios $\chi\sigma = D\sigma/D\sigma^\circ$ where $D\sigma = \tau\sigma - \nabla s - \frac{1}{4}(\nabla\rho\sigma)^2/\rho\sigma$ and $D\sigma^\circ = 3/5(6\pi^2)^{2/3}\rho\sigma^{5/3}$ correspond respectively to a measure of Pauli repulsion ($D\sigma$) of the actual system and to the free electron gas repulsion ($D\sigma^\circ$) and $\tau\sigma$ is the kinetic energy density. The ELF function is normalized between 0 (zero localization, blue areas) and 1 (strong localization, red areas) with the value of 1/2 corresponding to a free electron gas behavior. Fig. 2 shows two ELF contour plots for a horizontal plane at z = 1/2 containing Li and Si2 and a vertical plane with Li, Si1 and Y. Whereas there is a nearly free electron like behavior (green) between Li and Si2, the large red contours around Si2 and the blue ones around Li indicate a large electron localization around Si and little around Li. This is also shown in the vertical plane plot with Si1 in the neighborhood of Li for two adjacent cells along the hexagonal *c* axis. Looking along the Li–Si1–Li direction the flattening of the Si contours in the neighborhood of Li is a signature of the Si1–Li bonding. Further the distortion of the ELF contours around Si1 towards Y and vice versa in both panels indicates the chemical interaction between them as it will be shown in the next sections.

In order to better assess these features, we analyzed the charge density issued from the self consistent calculations using the AIM (atoms in Molecules theory) approach [37] developed by Bader who devised an intuitive way of dividing molecules into atoms as based purely on the electronic charge density. Typically in chemical systems, the charge density reaches a minimum between atoms and this is a natural region to separate atoms from each other. Such an analysis can be useful when trends between similar compounds are examined; however they do not constitute a tool for evaluating absolute ionizations. Further in order to include core electrons within the PAW method, use is made of the LAECHG = .TRUE. parameter in INCAR [19,20]; then we operate a summation of core and valence charge densities using a simple *perl* program. The computed charge changes ΔQ results are such as: Li: +1; Y: +1.39, Si1: −2.62 and Si2: −2.28 with an average ΔQ(Si): −2.39, leading to neutral LiYSi. The larger charge on Si1 arises from Li and results from the closer Li–Si1 neighborhood versus Li–Si2 (Fig. 1). The departure of the valence electron from Li towards Si, not Y, is also observed from different computations in $LiMO_2$ (M: transition metal) [35] and $LiTiS_2$ [38] where the electron transfer is towards O/S, not to *M*. This is also in agreement with the Pauling electronegativities χ = 0.98, 1.22, 1.9, resp. for Li, Y and Si whereby Li is the most electropositive on one hand and indicates covalent Y–Si bonding due to the small difference between their electronegativities. Similar calculations of charge changes in YSi give ΔQ(Y) = 1.28 and ΔQ(Si) = −1.28, signaling a larger covalent character with respect to LiYSi. The charges calculated for LiYSi compare well with those recently calculated for the binary lithium silicides [39].

4. Electronic structure and chemical bonding

In as far as the optimized lattice parameters are in good agreement with experiment we use the latter (Table 1) to analyze the electronic structure and the chemical bonding using all electrons calculations with the full potential ASW method. The site projected density of states (PDOS) for both LiYSi and YSi are shown in Fig. 3. Due to the vanishingly small density of states (DOS) at the top of the valence band (VB) in LiYSi, the zero energy along the

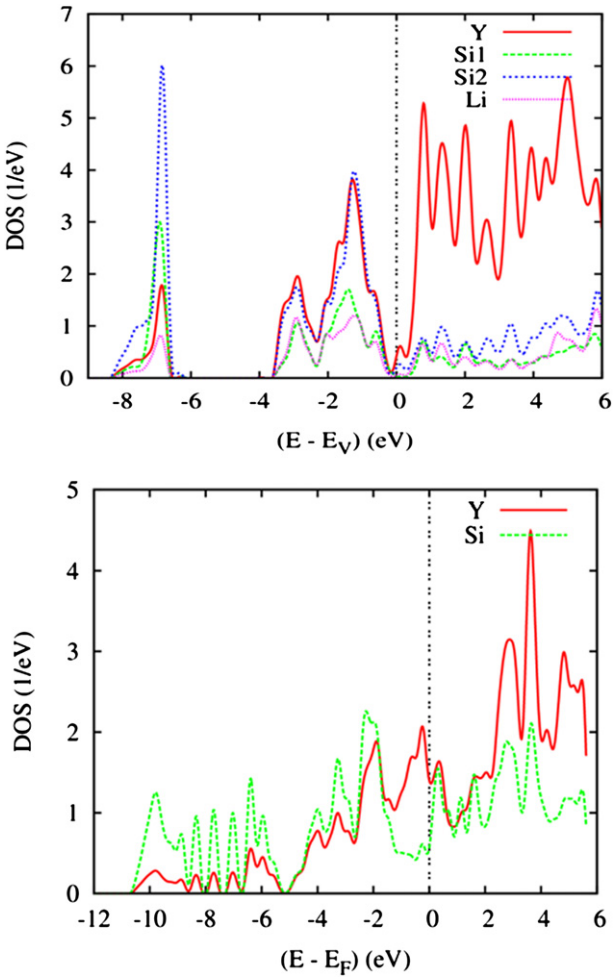

Fig. 3. Site projected density of states (PDOS) for LiYSi (top) and YSi (bottom).

x-axis is with respect to E_V and the compound is semi-conducting with a small gap. On the contrary, YSi which exhibits a finite DOS at the top of the VB is a metal and has the zero energy along the x-axis at the Fermi level (E_F). The difference in the DOS between the two compounds is also in their relative localizations. In LiYSi there is a separation of 2 eV between the s-like PDOS block centered at −7 eV and the p-like block in the range {∼ −4 eV, E_V}. Yttrium d states are found centered in the conduction band (CB) since Y is at the beginning of the 2nd period with an empty d subshell. YSi on the contrary is characterized by a continuous broad valence band extending over a range of 10 eV. In both compounds the constituents PDOS show similar shapes, translating the hybridization (quantum mixing) between the valence states of the basis sets. This translates a chemical bonding which we analyze with the overlap populations using the COOP approach.

Fig. 4 shows the COOP for LiYSi in two panels accounting for all species (3 of each kind) on one hand (top) and considering one species of each kind in Fig. 3b on the other hand. This explains the difference of scales along the y-axis. For both panels, the whole range of the VB is of bonding character (positive COOP). The lower part of the VB below −4 eV with s-like states shows no significant bonding in as far as such s orbitals are non directional; the main bonding involves p (Li, Si) and d (Y) states; the p contribution for Li being brought by its interaction with Si. As suggested in the introduction the weakest bonding is for Li–Y and the strongest one for Y–Si which ensures for the structural stability, i.e. the structure could be stable upon removing Li. Intermediate bonding is observed for Li–Si with much weaker intensity than Y–Si. Due to the different Si1/Si2 Wyckoff sites we detail furthermore the bonding in Fig. 3 (lower panel) which shows the same trends as in Fig. 3a with, however, more details such as the larger Li–Si1 and Y–Si2 bonding versus Li–Si2 and Y–Si1. This results from distances d(Li–Si1) = 265 pm versus d(Li–Si2) = 278 pm and could enable Li de-intercalation at different stages starting with the breaking of the weaker Li–Si2 bonds.

Fig. 5 shows the COOP for YSi in its experimental structure (top) and in the hypothetic Li-free one (bottom) calculated with the lattice parameters from Table 1. From the upper panel, the bonding also occurs in the higher energy part of the VB with dominant Y–Si bonding and less intense Si–Si mainly from −5 to −2 eV. Due to the low filling of Y valence states, the bonding character of Y–Si extends far within the CB. Then the stability of YSi is ensured by both Y–Si and Si–Si bonding interactions with a slight antibonding character for the latter. Different features appear for $\square_{Li}$YSi (bottom) with sharper COOP peaks and a larger bonding Y–Si and antibonding Si–Si contribution at the top of the VB thus exhibiting ionic like features imposed by the structure despite the absence of lithium. However the characteristics of mainly bonding Y–Si are present. Nevertheless the large antibonding Si–Si interaction within the VB is destabilizing to the compound; it further mirrors the lower stability of YSi in the hexagonal structure of LiYSi as shown in Table 1 from the absolute energy values.

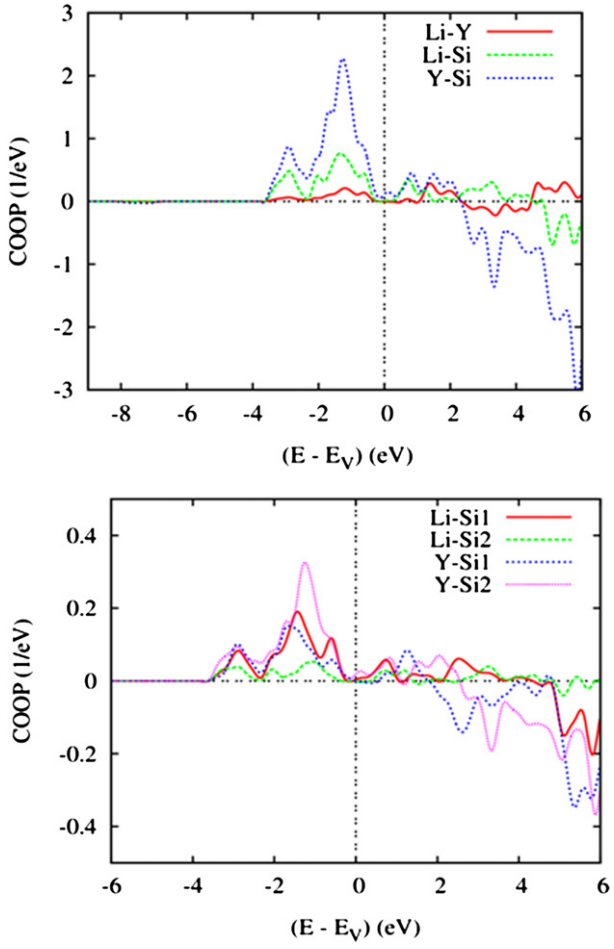

Fig. 4. Chemical bonding for pair interactions in LiYSi for all atom multiplicities (top) and for atom-to-atom COOP (bottom).

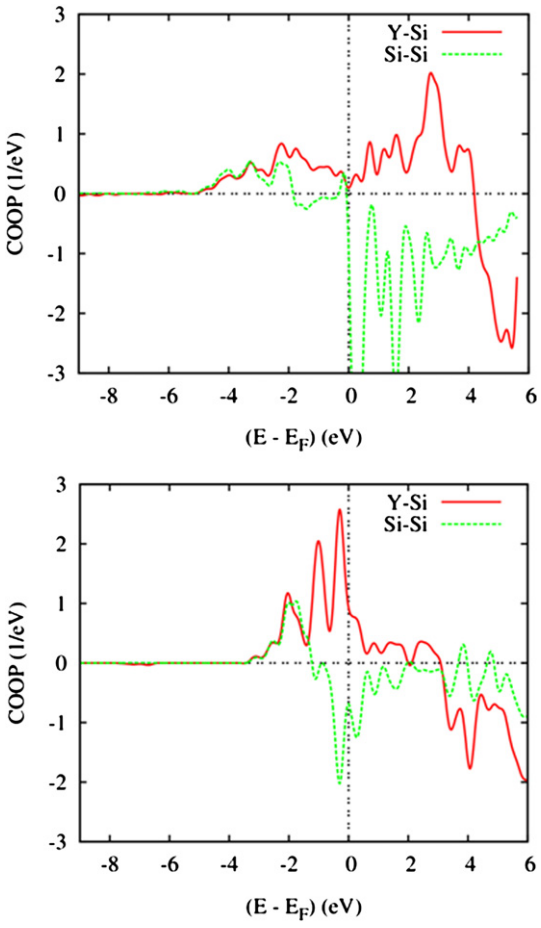

Fig. 5. Chemical bonding for pair interactions in YSi in the experimental structure (top) and in hypothetic Li-free LiYSi (bottom).

5. Conclusions

Electronic structure calculations of the electron precise Zintl phase LiYSi ($\equiv Li^{+}Y^{3+}Si^{4-}$) show semi-conducting behavior with a very small gap. The main bonding interactions were found mainly between Y and Si as well as Li–Si with a clear differentiation Li–Si1/Li–Si2 for the two crystallographically independent silicon sites. The electronic structure calculations indicate the possibility of an at least partial delithiation $Li_{1-x}YSi$ while keeping the hexagonal structure. A totally de-intercalated model compound keeping the hexagonal YSi substructure with a reduced c/a ratio and a smaller cell volume was found less stable than the experimentally observed binary silicide YSi with orthorhombic CrB type structure. Experimental investigations are underway.

Acknowledgments

This work was financially supported by the Deutsche Forschungsgemeinschaft (PAK 177) and the Bundesministerium für Forschung und Technologie (LiVe – Lithium-Verbundstrukturen within the programme LIB 2015). Support from the Centre Supérieur de la Recherche (CSR)-USEK-Lebanon is also gratefully acknowledged.

References

[1] U. Kasavajjula, C. Wang, A. John Appleby, J. Power Sources 163 (2007) 1003.
[2] M.N. Obrovac, L.J. Krause, J. Electrochem. Soc. 154 (2007) A103.
[3] Y. Kubota, M.C. Sison Escaño, H. Nakanishi, H. Kasai, J. Appl. Phys. 102 (2007) 053704.
[4] A. Kuhn, P. Sreeraj, R. Pöttgen, H.-D. Wiemhöfer, M. Wilkening, P. Heitjans, J. Am. Chem. Soc. 133 (2011) 11018.
[5] A. Kuhn, P. Sreeraj, R. Pöttgen, H.-D. Wiemhöfer, M. Wilkening, P. Heitjans, Angew. Chem. 123 (2011) 12305.
[6] S. Dupke, T. Langer, R. Pöttgen, M. Winter, H. Eckert, Solid State NMR 40, in press.
[7] R. Pöttgen, T. Dinges, H. Eckert, P. Sreeraj, H.-D. Wiemhöfer, Z. Phys. Chem. 224 (2010) 1475.
[8] T. Dinges, U. Ch. Rodewald, S.F. Matar, H. Eckert, R. Pöttgen, Z. Anorg. Allg. Chem. 635 (2009) 1894.
[9] G. Steinberg, H.-U. Schuster, Z. Naturforsch 34b (1979) 1237.
[10] A. Czybulka, G. Steinberg, H.-U. Schuster, Z. Naturforsch 34b (1979) 1057.
[11] V.V. Pavlyuk, V.K. Pecharskii, O.I. Bodak, Dopov. Akad. Nauk. Ukr. RSR, Ser. B 2 (1989) 50.
[12] Q. Xie, R. Nesper, Z. Anorg. Allg. Chem. 632 (2006) 1743.
[13] V.V. Pavlyuk, O.I. Bodak, Russ. Metall. 2 (1993) 181.
[14] V.V. Pavlyuk, V.K. Pecharskii, O.I. Bodak, V.A. Bruskov, Sov. Phys. Crystallogr. 33 (1988) 24;
Kristallografiya 33 (1988) 46.
[15] F. Merlo, A. Palenzona, M. Pani, S.K. Dhar, R. Kulkarni, J. Alloys Compd. 394 (2005) 101.
[16] T. Langer, S. Dupke, H. Eckert, S. F. Matar, M. Winter, R. Pöttgen, Solid State Sci., in press.
[17] P. Hohenberg, W. Kohn, Phys. Rev. 136 (1964) B864.
[18] W. Kohn, L.J. Sham, Phys. Rev. 140 (1965) A1133.
[19] G. Kresse, J. Furthmüller, Phys. Rev. B 54 (1996) 11169.
[20] G. Kresse, J. Joubert, Phys. Rev. B 59 (1999) 1758.
[21] P.E. Blöchl, Phys. Rev. B 50 (1994) 17953.
[22] J. Perdew, K. Burke, M. Ernzerhof, Phys. Rev. Lett. 77 (1996) 3865.
[23] W.H. Press, B.P. Flannery, S.A. Teukolsky, W.T. Vetterling, Numerical Recipes, Cambridge University Press, New York, 1986.
[24] M. Methfessel, A.T. Paxton, Phys. Rev. B 40 (1989) 3616.
[25] H.J. Monkhorst, J.D. Pack, Phys. Rev. B 13 (1976) 5188.
[26] A.R. Williams, J. Kübler, C.D. Gelatt, Phys. Rev. B 19 (1979) 6094.
[27] V. Eyert, The Augmented Spherical Wave Method – A Comprehensive Treatment, Lecture Notes in Physics, Springer, Heidelberg, 2007.
[28] R. Hoffmann, Angew. Chem. Int. Ed. Engl. 26 (1987) 846.
[29] J. Emsley, The Elements, Clarendon Press, Oxford, 1989.
[30] R. Nesper, Prog. Solid State Chem. 20 (1990) 1.
[31] J. Donohue, The Structures of the Elements, Wiley, New York, 1974.
[32] T. Dinges, R.-D. Hoffmann, R. Pöttgen, Z. Naturforsch 65b (2010) 537.
[33] E. Parthé, Acta Crystallogr. 12 (1959) 559.
[34] D.M. Ceperley, B.J. Alder, Phys. Rev. Lett. 45 (1980) 566.
[35] M.K. Aydinol, A.F. Kohan, G. Ceder, K. Cho, J. Joannopoulos, Phys.Rev. B 56 (1997) 1354.
[36] A.D. Becke, K.E. Edgecombe, J. Chem. Phys. 92 (1990) 5397.
[37] R. Bader, Chem. Rev. 91 (1991) 893.
[38] C. Umrigar, D.E. Ellis, Ding-Sheng Wang, H. Krakauer, M. Posternak, Phys. Rev. B 26 (1982) 4935.
[39] V.L. Chevrier, J.W. Zwanziger, J.R. Dahn, J. Alloys Compd. 496 (2010) 25.